A two-dimensional manganese-containing coordination polymer for efficient catalysis of the oxygen evolution

Shaista Ibrahim,[1] Muhammad Mohsin Saleem,[1] Muhammad Imran,[1] Waqas Ali Shah,[1] David. B. Cordes,[2] Alexandra M. Z. Slawin,[2] Muhammad Arif Nadeem [1]*

[1] Catalysis and Nanomaterials Lab 27, Department of Chemistry, Quaid-I-Azam University, Islamabad 45320, Pakistan

[2] EaStCHEM School of Chemistry, University of St Andrews, St Andrews, Fife KY16 9ST, U. K.

M.A.N; manadeem@qau.edu.pk, +92-51-9064-2062

Abstract

The structural stability of coordination polymers is very important to act as efficient catalysts. A novel two dimensional manganese based coordination polymer $[Mn_2(ox)(sqr)(dmso)_2]_n$ (**Mn-CP**) {ox = oxalate, sqr = squarate, dmso = dimethylsulfoxide} has been fabricated, keeping in consideration that the extensive delocalization of π-electron densities of both non-innocent redox active ligands will make a manganese an efficient oxygen-evolving centre by improving its poor intrinsic conductive nature. **Mn-CP** has displayed excellent OER performance at neutral pH, exhibiting a current density (**J**) of 10 mA/cm^2 at an overpotential (**η**) of 300 mV (*vs*. RHE), with a Tafel slope (**TS**) of 82.4 mV/dec in PBS (pH = 7.4). The enhanced water oxidizing ability can be credited to the unique two-dimensional planer-conducting layers of oxalates and squarates with Mn^{2+} ions. FT-IR, PXRD and controlled potential electrolysis (CPE) investigate that **Mn-CP** stays functional and structurally intact for a period of 10 hours.

Keywords: Manganese; coordination polymer; water oxidation; overpotential; Tafel slope

Introduction

Electrochemical water splitting can be a feasible method to generate hydrogen which involves oxygen and hydrogen evolution at anode and cathode, respectively. The oxygen evolution reaction (OER) is particularly problematic for the generation of hydrogen as it involves various proton-integrated electron movement ($4H^+/4e^-$) processes. [1].

Precious metals (Ir, Ru and Pt) and metal oxides have been expended as touchstone OER electrocatalysts on account of their efficient kinetics for oxygen evolution process. However, their large price, disintegration in acidic and alkaline media respectively, render their deployment unfeasible at the industrial level [2, 3]. From this perspective, the exploration of an inexpensive, proficient and robust electrocatalyst that work under neutral environments have enticed greater interest owing to the benefits of low causticity/corrosion problems and copious neutral water sources [4].

Inspired from the natural photosynthetic system, manganese (Mn) based catalysts such as MnO/C composites and Mn-based metal organic frameworks (MOFs) have recently been utilized in OER applications [5-7]. A sub-class of coordination polymers (CPs), metal-organic frameworks (MOFs), are presented as auspicious water oxidation catalysts, with the possibility to utilize their adjustable assemblies, large surface area, variable functionalities, high porosity and numerous active sites [8-11]. In MOFs, uniformly distributed metal nodes serve as active catalytic sites by virtue of their redox properties being tuned by the organic linkers. The linkers also reduce the resistance of the system as well as offering greater anodic catalytic hotspots, therefore augmenting the structural and performance stability of MOFs as electrode materials [12-14].

Various manganese oxides have been utilized as electrocatalysts for OER. Recently, Liu et al developed MnO/C nanorods by the thermal decomposition of Mn-MOF-74 and produced twice the current density (20 mA/cm^2) with almost the same overpotential (η = 329 mV) in

electrochemical water oxidation studies but they achieved this double current density by the **thermal decomposition of Mn-MOF-74 in 1 M KOH (pH≈13/14)** [15]. Similarly, MnO_2 nanowires produced the same current density (J = 10 mA/cm^2) with less overpotential (η = 262 mV) inside the pores of **Ni MOF in 1 M KOH (pH≈13/14)** [16]. The electrochemical measurements demonstrated that the possible **sy**nergistic effect of Ni MOF and MnO_2 nanowires to OER activity and the presence of pyridine N and Ni^{3+} are also the factors which could help facilitating the performance of OER whereas **Mn-CP** produced a current density (J) of 10 mA/cm^2 at an overpotential (η) of 300 mV **at neutral pH (pH = 7.4) in as synthesized form without the thermal decomposition of the polymer.**

In another study, a hollow Mn_2O_3 nanotube array was prepared by calcining the same Mn-MOF at different temperatures. However, in water oxidation reactions, Mn_2O_3 in alkaline medium produced **J** = 10 mA/cm^2 at **η** = 270 mV having **TS** = 85 mV/dec [17].

Another approach involves incorporation of manganese oxide into the porous structure of MOFs. Lin et al improved the structural stability of MIL-101(Cr) by assembling α-MnO_2 nanoparticles inside the pores by hydrothermal synthesis, which bring about an enhanced electrochemical activity in water oxidation studies [18]. However, the poor inherent conductivity of MnO_2 i.e. 10^{-5}-10^{-6} S.cm^{-1} has restricted its utilization in direct power applications [19]. Very recently, Butt et al used Mn-based CP $\{[Mn(ox)_{3/2}][bap].(H_2O)\}_n$ as water oxidation electrocatalyst and obtained **J** = 10 mA/cm^2 in 0.1 M KOH solution as a consequence of large **η** value i.e. = 404 mV having high **TS** value = 399 mV/dec [20]. The structural design or choice of ligands within an electrocatalyst strongly influences their catalytic behaviour. It was found that squarate and oxalate based polymers have shown better thermal, conductive and electrochemical properties due to highly conducting layers of these ligands [21].

Herein, the poor conductive nature of MnO_2 is overcome by constructing a novel manganese based coordination polymer, $[Mn_2(ox)(sqr)(dmso)_2]_n$ (**Mn-CP**), by assembling highly conductive and electron donating oxalate and squarate linkers with Mn^{2+}. The **Mn-CP** was studied by linear sweep voltammetry (LSV), chronoamperometry (C.A), and controlled potential electrolysis (CPE) to investigate various electrocatalytic water oxidation parameters (overpotential, Tafel slope, TOF and stability). **Mn-CP** exhibit **J** = 10 mA/cm^2 with a **TS** = 82.4 mV/dec at **η** = 300 mV in neutral conditions (pH = 7.4). To the best of our information, no manganese-based CP has been used as a water oxidation catalyst at neutral pH without calcining or pyrolyzing the CP.

Experimental

Preparation of $[Mn_2(ox)(sqr)(dmso)_2]_n$ (Mn-CP)

To a DMSO solution (5 mL) of $MnCl_2 \cdot 4H_2O$ (0.198 mg, 1 mmol), a mixture of oxalic acid trihydrate (0.07204 g, 0.5 mmol) and squaric acid (0.05703 g, 0.5 mmol) dissolved in DMF (5 mL) was added and the solution was stirred for 20 min. Following this, the solution was transferred to a glass vial that was sealed and heated at 90 °C in an oven for three days. The colourless crystals obtained after vacuum filtration were washed (by ethanol and DMSO) and dried. Anal. calcd. For $C_{10}H_{12}Mn_2O_{10}S_2$, C, 25.76 %; H, 2.59 %; S, 13.76 %. Found: C, 25.70 %; H, 2.53 %; S, 13.72 %. Selected FTIR (cm^{-1}): 3333 brs, 1637 m, 1489 intense, 1310 s, 1002 m, 967 s, 785 s, 718 s, 497 s, 414 s.

Preparation of Mn-CP coated FTO working electrode

A glass slide (area = 1× 2 cm^2) coated with fluorine-doped tin oxide (FTO) was first cleaned through agitating in saponaceous mixture, deionized water coupled with isopropanol, sequentially. The cleaned electrode was annealed in a furnace for one hour at 400 °C. The catalyst ink was formulated by adding **Mn-CP** (5 mg) to a mixture of analytical grade ethanol

(1.5 mL) and Nafion (25 μL) and sonicated for 3 h. The resulting ink was then drop cast onto the annealed FTO electrode, dried for the night at 70 °C and preserved in a desiccator afore conducting electrocatalytic water oxidation investigations.

Electrochemical measurements

Three-electrode system (a Pt wire as counter electrode, Ag/AgCl (3.0 M KCl) as reference electrode and a **Mn-CP** modified FTO as working electrode) was deployed to perform electrochemical studies under ambient conditions. Nernst equation (Eq. **1**) was used to convert potentials against reversible hydrogen electrode (RHE), which are recorded against Ag/AgCl reference electrode [22-24].

$$\mathbf{E_{RHE} = 0.1967 + 0.0592 \times pH + E_{Ag/AgCl}} \quad \text{(1)}$$

Where E_{RHE} is the transformed potential vs. RHE, $E_{Ag/AgCl}$ is the observed potential recorded against Ag/AgCl reference electrode, and 0.1967 is the standard potential of Ag/AgCl at 25 ^{o}C.

The pH of the solution was kept 7.4 by PBS tablets (one PBS tablet provides 137 mM NaCl, 2.7 mM KCl, 10 mM phosphate buffer solution and pH 7.4 in 200 mL water at 25 °C). The electrolytic solution was purged with N_2 gas for 30 minutes. Linear sweep voltammetry carried out in a potential window of 0-1.5 V *vs.* Ag/AgCl at a scan rate of 10 mV/s. Chronoamperometry was performed in the range of 0.7-1.35 V *vs.* Ag/AgCl with a difference of 0.02 V to measure overpotential and Tafel slope. Controlled potential electrolysis (CPE) was performed for 10 hours at a constant potential of 1.5 V *vs*. RHE.

Results and discussion

Single crystal XRD investigation

Selected crystallographic data is presented in Table **1** while selected bond lengths and bond angles are depicted in Table **S1**. The structure of **Mn-CP** was found to adopt the space group

Pnnm, having an empirical formula of $[Mn_2(ox)(sqr)(dmso)_2]$, and an asymmetric unit of a half of a manganese, a quarter each of the oxalate and squarate, and half of the dmso. In **Mn-CP**, the oxalato ligand adopted a fascinating μ_4-bridging coordination approach and chelating to two Mn centres with an anisobidentate mode of attachment [Mn1-O1=2.255(18) Å and Mn1-O2=2.202(2) Å] by constructing two five membered Mn-O-C-C-O metallacyclic rings with bite angle of 73.95(7)°.

Table 1: Crystallographic parameters of **Mn-CP**

Mn-CP			
Empirical formula	$C_{10}H_{12}Mn_2O_{10}S_2$	Density / g cm^{-3}	1.881
Molecular weight	466.19	Reflections collected	8335
Crystal description	Colourless chip	Independent reflections	814
Crystal size / mm^3	0.03 × 0.01 × 0.01	R_{int}	0.0402
Crystal system	Orthorhombic	Parameters, restraints	78, 2
Space group	*Pnnm*	GoF on F^2	1.080
a / Å	18.8158(13)	R_1 (all data)	0.0267
b / Å	5.9111(4)	R_1 [$I \geq 2\sigma(I)$]	0.0246
c / Å	7.3983(5)	Volume / Å^3	822.85(10)
wR_2 (all data)	0.0635	wR_2 [$I \geq 2\sigma(I)$]	0.0625

This asymmetric binding mode for the oxalate moiety is also displayed in the oxalate C-O bonds, as a longer C-O bond [1.258(3) Å] is associated with the long Mn-O bond [2.255(18) Å] and likewise shorter bonds associating [C-O = 1.240(3) Å, Mn-O= 2.202(2) Å]. This may be due to variations in shifting of electron density from C-O toward metal centre. Additionally, it is worth noting that this oxalato moiety is further attached to two Mn centres via μ_2-O1 atoms in a *trans* manner such that an inversion centre lies in the middle of its C-C bond. The disparate attachment of both μ_2-O1 to two Mn centres [Mn1-O1=2.255(18), 2.198(18)] from opposite sides additionally fabricates four membered Mn1-O1-Mn1-O1 metallacyclic rings [Mn1-O1-

Mn1 angle = 103.73(7)°]. Thus, the bridging of the oxalato ligands between four metal centres generates a 1D polymeric chain along the *b*-axis, in which each Mn-atom adopts distorted octahedral geometry [MnO_6]. The equatorial plane of the manganese octahedron is defined by three coordination oxygens from two chelating oxalato ligand via two μ_2-O atoms and a monodentate oxygen, while the fourth position is occupied by the O-atom of coordinated DMSO. The deviation of O1-Mn1-O2 bond angle from ideality is due to small bite angle of the chelating oxalato ligand. The apical positions of the octahedron are occupied by the squarate ligand binding in a μ_4-isotetradentate manner. Thus, the squarate ligand links 1D chains of Mn-oxalate to fabricate a 2D network in the *bc*-plane having a rectangular grid topology (Figure 1a). The in-plane distance between Mn atoms bridged by oxalate was 7.40 Å and the distance between those bridged by squarate was 5.91 Å. Despite the apparent potential pores in these sheets, these are blocked by the offset stacking of adjacent sheets, such that the capping DMSO molecules protrude into the rectangular gaps within the sheets, filling them.

PXRD and TGA investigations

PXRD analysis was used to determine the purity of the **Mn-CP**. All the diffraction patterns of synthesized **Mn-CP** are in good agreement with the simulated one obtained from the single crystal data (Figure 1b).

Thermogravimetric studies of **Mn-CP** show no apparent mass loss up to about 350 °C, confirming the absence of any readily removed solvent moiety in the framework (Figure 1c). A sudden mass loss (about 58.2 %) occurred in the temperature range of 350-450 °C, suggesting the removal of organic components, giving MnO as a residue.

Electrocatalytic Water Oxidation Studies

Both oxalate and squarate exist in different canonical forms (Scheme S1). The extensive delocalization of π-electron density in these two organic linkers make them non-innocent redox

active ligands and further enables manganese to act as an efficient oxygen evolving centre not only by improving its inherently poor conductive nature but also by allowing switching of the +2 valence state of Mn into higher ones. Consequently, the Mn ions remain firmly bound in the 2-D coordination polymer in different stages of electrochemical water oxidation processes. The existence of oxygen atoms in the first coordination sphere retards the rate of catalyst disintegration [25, 26].

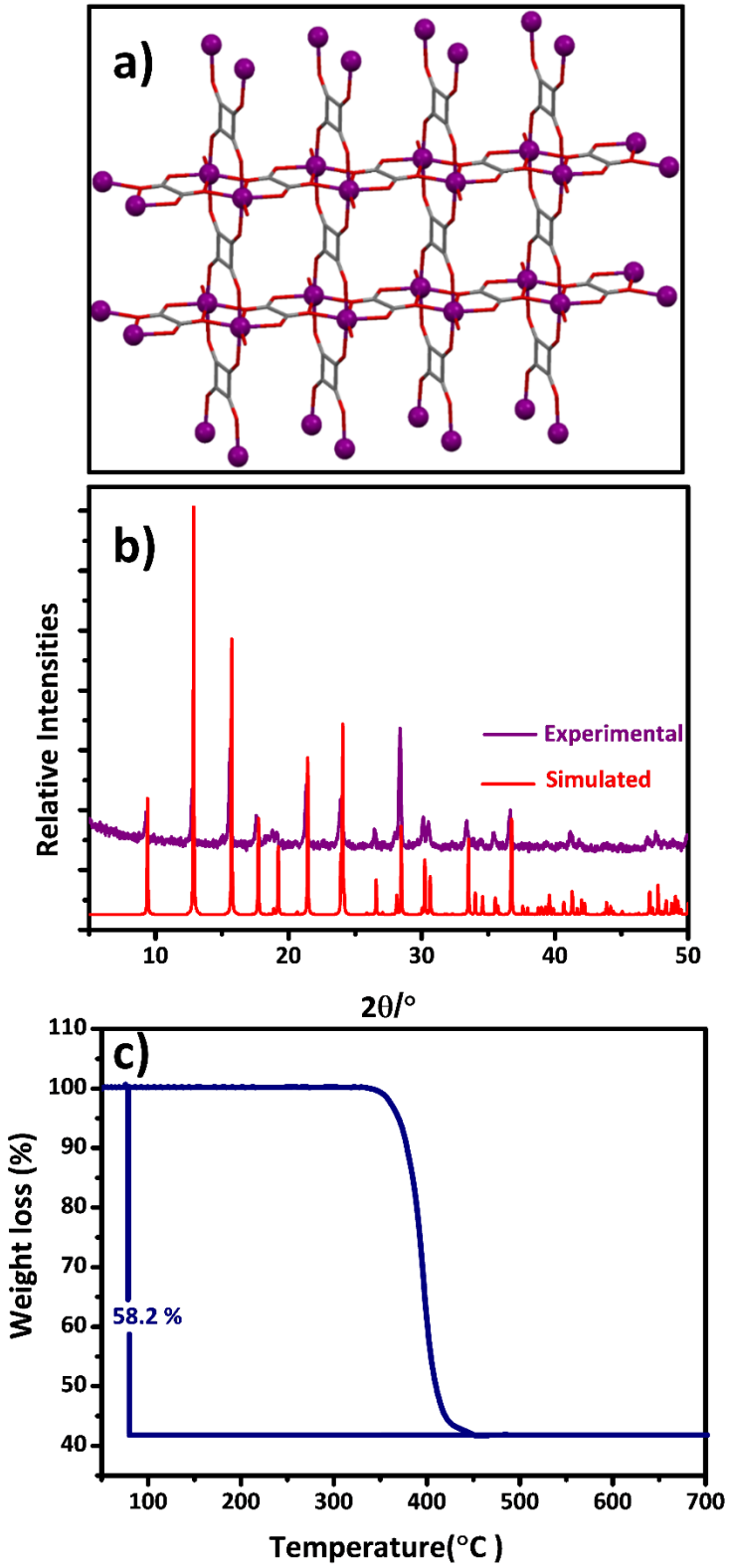

Figure 1: a) View of a section of one sheet of **Mn-CP** viewed lying in the *bc*-plane. (Mn = violet, O = red and C = grey). DMSO molecules (except oxygen) have been omitted for clarity. b) Comparison of a simulated and observed pattern of **Mn-CP**. c) Thermogram of **Mn-CP**.

Linear sweep voltammetry of a **Mn-CP** coated modified FTO electrode shows a significant rise in the current at 1.3 V *vs*. RHE, attributable to catalytic oxygen evolution (Figure 2a). The chronoamperometry measurements are carried out over a voltage range of 100 – 260 mV *vs.* RHE that displayed a straight line trend between the overpotential (**η)** and log of current density (J). Comparison of the electrocatalytic performance of **Mn-CP** with that of reported Mn based electrocatalysts (Table 2) indicates that **Mn-CP** has promising water oxidation kinetics. The Tafel slope of the **Mn-CP** coated FTO electrode, obtained from log(j) *vs*. **η**, was found to be 82.4 mV/dec (Figure 2b). This value of Tafel slope is lower than those of the reported Mn_2O_3 nanoarrays (85 mV/dec) [17], dandelion-like α-MnO_2 (155 mV/dec) [27], urchin-like α-MnO_2 (210 mV/dec) [27], prismatic α-Mn_2O_3 (146 mV/dec) [28], MnOx (120 mV/dec) [29] and higher than those of the Ni-MOF–MnO_2 composite nanoparticles-nanowires (69.46 mV/dec) [16], MnO_2-KIT-6 hexagonal-pore nanostructure (60 mV/dec) [30], Mn-CoP nanosheets (76 mV/dec) [31], CoMnP nanoparticles (61 mV/dec) [32], porous α-Mn_2O_3 (50 mV/dec) [33], Mncat (80 mV/dec) [34] and MnO/C nanorod arrays (70.02 mV/dec) [15]. In order to obtain **J** = 1 mA/cm^2, the required overpotential is 218 mV (*vs*. RHE), which is quite low as compared to δ-MnO_2 (**η** = 724 mV) [35], MnPi (**η** = 563 mV) [36], Mn_5O_8 (**η** = 550 mV) [37], MnO_x (**η** = 485 mV) [29], Mn_2Ln_2 (Ln = Dy, Gd; **η** = 880 mV) [38] and Mncat catalysts (**η** = 590 mV) [34]. In order to attain a current density of 10 mA/cm^2, the overpotential required was 300 mV (*vs.* RHE), which is also quite low in comparison with those seen for MnO_2-KIT-6 hexagonal pore nanostructure (**η** = 610 mV) [30], Mn oxide (**η** = 1770 mV) [39], Mn_2O_3 at 450 °C (**η** = 387 mV) [40], β-manganese oxide (**η** = 500 mV) [41], dandelion-like α-MnO_2 (**η** = 550 mV) [27], urchin-like α-MnO_2 (**η** = 640 mV) [27], MnO-150 nm (**η** = 463 mV) [42], CoMnP nanoparticles (**η** = 330 mV) [32] and higher than Ni-MOF–MnO_2 composite nanoparticles-nanowires (**η** = 262 mV) [16], Mn_2O_3 nanoarrays (**η** = 270 mV) [17] and Mn-CoP nanosheets (**η** = 270 mV) [31]. The surface concentration of **Mn-CP** in the modified FTO electrode was

utilized to calculate the turn over frequency (TOF), see the Supporting Information for detail. In order to produce a TOF of 1.32×10^{-4} s^{-1}, an overpotential of 225 mV is required (Figure 2c), which is less than that of Mn polypods (**η** = 350 mV) [43].

To gain insight into the stability of the **Mn-CP** modified electrode**,** controlled potential electrolysis (CPE) was conducted at 1.5 V *vs*. RHE for a period of 10 hours. After a minor increase initially, the current density maintained at a constant value (Figure 3a). Inset in Figure 3a shows the images of **Mn-CP** modified FTO electrodes before and after catalytic performance.

The recoverability of the catalyst was assessed by performing comparative investigation of LSV, PXRD and FTIR patterns of pristine and post-catalytic **Mn-CP** modified electrodes (Figures 3b, 4a and 4b respectively). No considerable dissimilarities in LSV, PXRD and FTIR patterns of pristine and post-catalytic **Mn-CP** modified electrodes were seen, signifying the firmness and retention of catalyst after the oxygen evolution process.

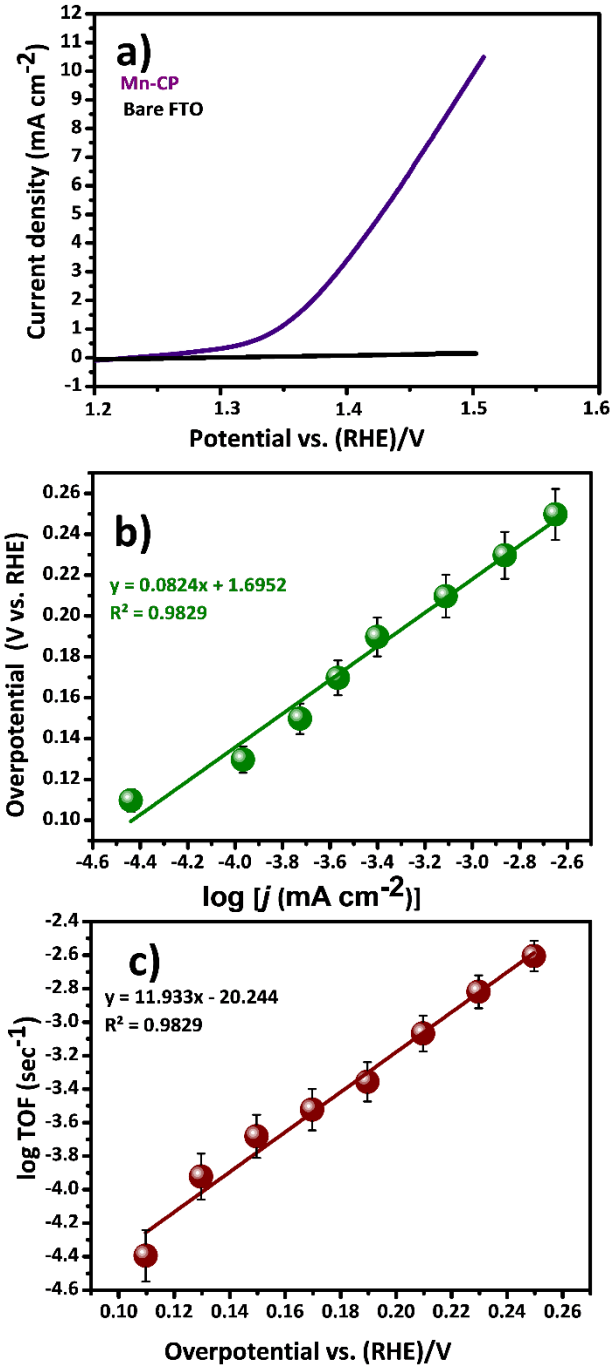

Figure 2: a) LSV of **Mn-CP** modified FTO electrode (violet) and the bare FTO (black) at scan rate of 10 mV s^{-1}. b) Plot of overpotential (**η**) as a function of log of current density (log(j)) to obtain tafel slope for **Mn-CP**. c) Plot of dependence of TOF of **Mn-CP** on overpotential (**η**) All electrochemical measurements are carried out in phosphate buffer saline solution (pH = 7.4)

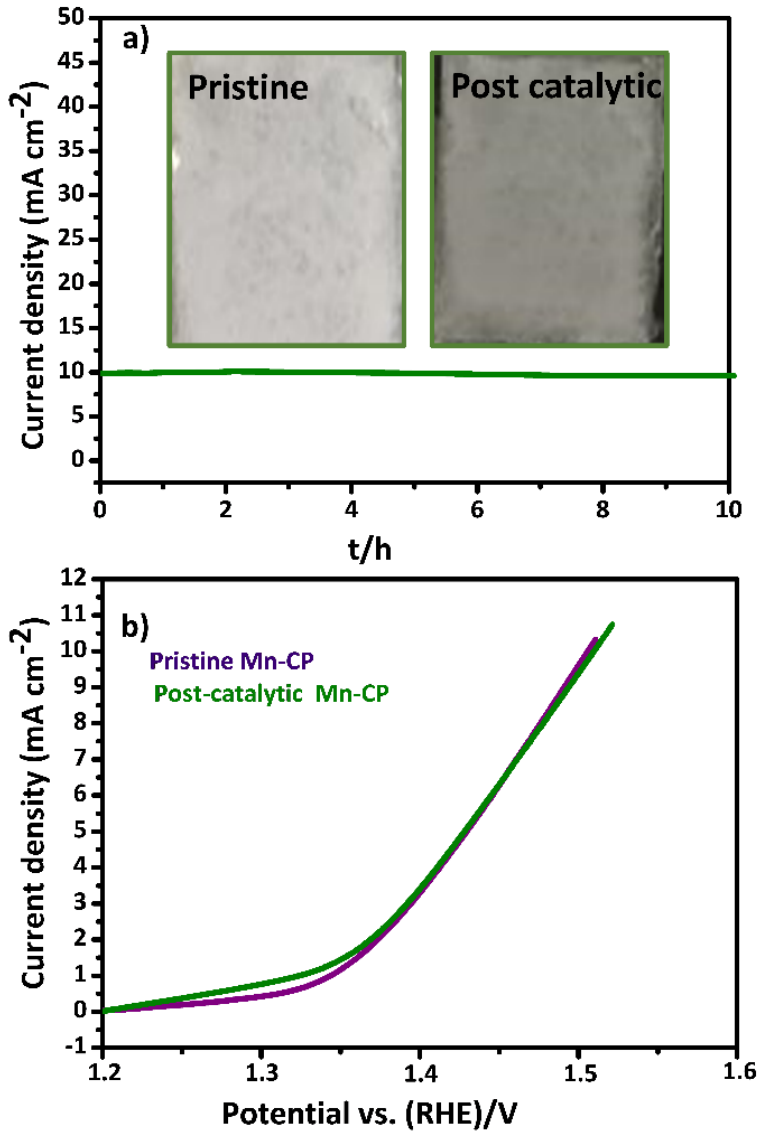

Figure 3: a) Bulk electrolysis of **Mn-CP** modified electrode at a constant voltage 1.5 V (*vs* RHE) for a period of 10 hours. Inset shows the images of **Mn-CP** modified FTO electrodes before and after catalytic performance. b) Linear sweep voltammograms (LSV) of pristine and post-catalytic **Mn-CP** modified electrodes. All electrochemical measurements are carried out in phosphate buffer saline solution (pH = 7.4)

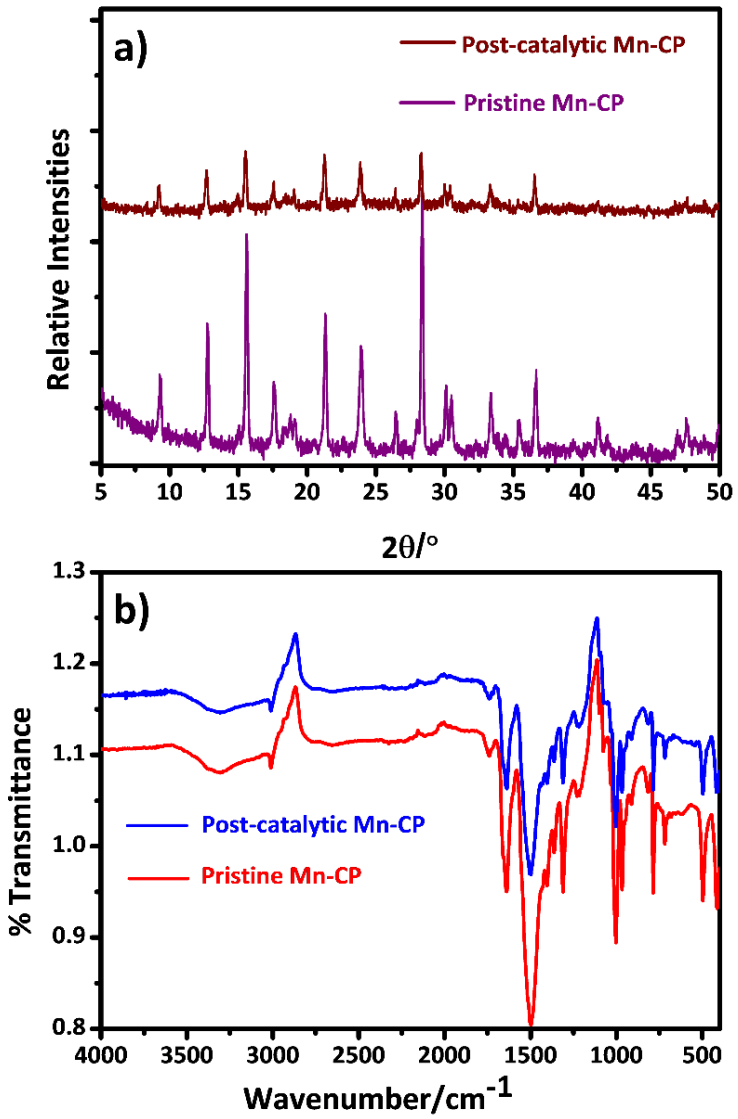

Figure 4: a) Comparative investigation of PXRD of pristine and post-catalytic **Mn-CP** modified electrodes b) Comparative investigation of IR spectra of pristine and post-catalytic **Mn-CP** modified electrodes.

Table 2: Summary of the electrocatalytic performance of **Mn-CP** with that of reported Mn based electrocatalysts.

Compound name	**Tafel slope (mV/dec)**	**(η) (mV)**	***I*** **(mA/cm^2)**	**Electrolyte**	**Substrate**	**Ref.**
Mn-CP	82.4	218 300	1 10	PBS	FTO	This study
IrO_2	61	470	10	1 M KOH	Au-RDE	2015 [44]
$\{[Mn(ox)_{3/2}][bap].(H_2O)\}_n$	399	404	10	0.1 M KOH	FTO	2020 [20]
Ni-MOF wrapped MnO_2 nanowires	69.46	262	10	1 M KOH	RDE	2018 [16]
MnPi	_	563	1	0.05 M PBS	GC	2019 [36]
MnO Nanoparticles	70.1-82.6	530	10	0.5 M PBS	FTO	2017 [42]
α-MnO_2/MIL-101(Cr) composite nanoparticles	_	900	22	0.1 M KOH	Carbon paper	2014 [18]
MnO_2	_	600	0.03	0.5 M Na_2SO_4	FTO	2012 [45]
Mn-CoP nanosheets	76	290	10	1 M KOH	GC	2018 [31]
α-Mn_2O_3 prisms	146	956	0.1	0.1 M KOH	GC	2016 [28]
MnO_2-KIT-6 hexagonal pore nanostructure	60	610	10	0.1 M KOH	GC	2018 [30]
CoMnP nanoparticles	61	330	10	1 M KOH	GC	2016 [32]
δ-MnO_2	-	724	1	0.5 M Na_2SO_4	FTO	2012 [35]
Mn_2O_3 NAs	85	270 320	10 20	1 M KOH	Ni foam	2019 [17]
$Mn_3(PO_4)_2$	_	680	0.316	0.5 M PBS	FTO	2014 [46]
$LiMnP_2O_7$	_	680	0.5	0.5 M PBS	FTO	2014 [47]
Mn_5O_8	_	550	1	0.3 M PBS	FTO	2015 [37]
MnOx	_	330	1	1.0 M PBS	FTO	2017 [48]
MnO nanocatalysts	149	580	10	0.1 M KOH	RDE	2015 [43]
α-MnO_2 dandelion-like	155	550	10	0.1 M KOH		2017 [27]
α-MnO_2 urchin-like	210	640	10	0.1 M KOH		2017 [27]
Porous α-Mn_2O_3	50	340	8	1 M KOH	FTO	2017 [33]
MnO_x/CNT	_	570	8	0.1 M PPB	GC	2012 [49]
β-manganese oxide	_	500	10	1 M NaOH	FTO	2013 [41]
Mn_2O_3 (at 450 °C)	69.3	387	10	1 M NaOH	FTO	2016 [40]
MnO/C nanorod arrays	70.02	329 300	20 10	1 M KOH	Ni foam	2018 [15]
Mn_2Ln_2 (Ln = Dy, Gd)	_	880	1	PBS	FTO	2018 [38]
MnOx	120	485	1	0.1 M PBS	ITO	2013 [29]
Mncat	80	590	1	0.1 M PBS	ITO	2012 [34]

η = Overpotential, ***I***= Current density

Conclusions

A novel two dimensional manganese based coordination polymer $[Mn_2(ox)(sqr)(dmso)_2]_n$ (**Mn-CP**) has been prepared by solvothermally reacting oxalic acid and squaric acid organic linkers with $MnCl_2 \cdot 4H_2O$ in a DMSO/DMF solvent mixture. The new material was characterized by various techniques including single crystal XRD, PXRD, FTIR and TGA studies. A **Mn-CP** modified FTO electrode displayed excellent performance in water oxidation studies at pH = 7.4, requiring **η** = 300 mV *vs.* RHE to attain a **J** = 10 mA/cm^2, with a **TS** = 82.4 mV/dec, lower than many known water oxidation electrocatalysts. An overpotential of only 225 mV *vs.* RHE is required to produce a TOF of 1.32×10^{-4} s^{-1}. This high performance can be credited to the unique two dimensional planer conducting layers of oxalates and squarates in the crystalline coordination polymer whose highly conjugating π-electron densities make manganese an efficient oxygen evolving centre by improving its poor intrinsic conductive nature and by allowing it the flexibility to achieve higher oxidation states. Controlled potential electrolysis (CPE) was conducted at a constant voltage 1.5 V (*vs* RHE) for a period of 10 hours in which current density remained constant without any change. Comparative investigations of PXRD and FTIR plots showed no divergences of pristine **Mn-CP** modified electrodes with those of post-catalytic electrodes, representing the stability and remanence of crystal structure after the oxygen evolution process. This study opens a new path of fabricating cutting edge robust and proficient water oxidation catalyst centred on metals having high natural reserves.

Acknowledgements

The work was financially supported by the Higher Education Commission (HEC) of Pakistan (No. 8400/Federal/NRPU/R&D/HEC/2017). This work was also supported by Alexander von Humboldt (AvH) Foundation, Germany, for return fellowship (Ref 3.5 - 1161601 - PAK - GFHERMES-P) awarded to M.A. Nadeem.

References

[1] W.A. Shah, S. Mir, S. Abbas, S. Ibrahim, L. Noureen, A. Kondinski, D.R. Turner, P. Kögerler, M.A. Nadeem, Robust and efficient electrocatalyst for water oxidation based on 4, 4′-oxybis (benzoate)-linked copper (II) hydroxido layers, Inorg. Chim. Acta 497 (2019) 119080.

[2] K. Klyukin, A. Zagalskaya, V. Alexandrov, Role of dissolution intermediates in promoting oxygen evolution reaction at RuO_2 (110) surface, J. Phys. Chem. C 123 (2019) 22151-22157.

[3] M. Batool, S. Ibrahim, B. Iqbal, S. Ali, A. Badshah, S. Abbas, D.R. Turner, M.A. Nadeem, Novel cobalt-fumarate framework as a robust and efficient electrocatalyst for water oxidation at neutral pH, Electrochim. Acta 298 (2019) 248-253.

[4] J. Wu, Y. Xue, X. Yan, W. Yan, Q. Cheng, Y. Xie, Co_3O_4 nanocrystals on single-walled carbon nanotubes as a highly efficient oxygen-evolving catalyst, Nano Res. 5 (2012) 521-530.

[5] D. Ji, H. Zhou, J. Zhang, Y. Dan, H. Yang, A. Yuan, Facile synthesis of a metal–organic framework-derived Mn_2O_3 nanowire coated three-dimensional graphene network for high-performance free-standing supercapacitor electrodes, J. Mater. Chem. A 4 (2016) 8283-8290.

[6] S. Maiti, A. Pramanik, S. Mahanty, Electrochemical energy storage in Mn_2O_3 porous nanobars derived from morphology-conserved transformation of benzenetricarboxylate-bridged metal–organic framework, CrystEngComm 18 (2016) 450-461.

[7] K. Zhao, K. Lyu, S. Liu, Q. Gan, Z. He, Z. Zhou, Ordered porous Mn_3O_4@ N-doped carbon/graphene hybrids derived from metal–organic frameworks for supercapacitor electrodes, J. Mater. Sci. 52 (2017) 446-457.

[8] S. Ibrahim, I. Majeed, E. Hussain, A. Badshah, Y. Qian, D. Zhao, D.R. Turner, M.A. Nadeem, Novel photo-functional material based on homo-metallic cyanide bridged nickel

coordination polymer and titania for hydrogen generation, Inorg. Chim. Acta 486 (2019) 684-693.

[9] S. Ibrahim, I. Majeed, Y. Qian, A. Iqbal, D. Zhao, D.R. Turner, M.A. Nadeem, Novel hetero-bimetallic coordination polymer as a single source of highly dispersed Cu/Ni nanoparticles for efficient photocatalytic water splitting, Inorg. Chem. Front. 5 (2018) 1816-1827.

[10] S. Ibrahim, U. Rafique, M. Saleem, W. Iqbal, S. Abbas, W.A. Shah, M. Imran, M.A. Nadeem, High performance of homo-metallic tetracyanonickelate based coordination polymer towards water oxidation electrocatalysis, Inorg. Chim. Acta 526 (2021) 120510.

[11] W.A. Shah, S. Ibrahim, S. Abbas, L. Naureen, M. Batool, M. Imran, M.A. Nadeem, Nickel containing polyoxometalates incorporated in two different metal-organic frameworks for hydrogen evolution reaction, J. Environ. Chem. Eng. 9 (2021) 106004.

[12] X. Zou, Y. Liu, G.D. Li, Y. Wu, D.P. Liu, W. Li, H.W. Li, D. Wang, Y. Zhang, X. Zou, Ultrafast Formation of Amorphous Bimetallic Hydroxide Films on 3D Conductive Sulfide Nanoarrays for Large-Current-Density Oxygen Evolution Electrocatalysis, Adv. Mater. 29 (2017) 1700404.

[13] L. Xie, C. Tang, K. Wang, G. Du, A.M. Asiri, X. Sun, $Cu(OH)_2$ @ $CoCO_3(OH)_2 \cdot nH_2O$ core–shell heterostructure nanowire array: an efficient 3D anodic catalyst for oxygen evolution and methanol electrooxidation, Small 13 (2017) 1602755.

[14] D.T. Genna, A.G. Wong-Foy, A.J. Matzger, M.S. Sanford, Heterogenization of homogeneous catalysts in metal–organic frameworks via cation exchange, J. Am. Chem. Soc. 135 (2013) 10586-10589.

[15] P.-P. Liu, H.-L. Zhu, Y.-Q. Zheng, Hybrid MnO/C nanorod arrays derived from a MOF precursor with enhanced oxygen evolution activity, J. Mater. Sci. 53 (2018) 11574-11583.

[16] Y. Han, Y. Yu, L. Zhang, L. Huang, J. Zhai, S. Dong, Facile synthesis of Ni based metal-organic frameworks wrapped MnO_2 nanowires with high performance toward electrochemical oxygen evolution reaction, Talanta 186 (2018) 154-161.

[17] P.-P. Liu, Y.-Q. Zheng, H.-L. Zhu, T.-T. Li, Mn_2O_3 hollow nanotube arrays on Ni foam as efficient supercapacitors and electrocatalysts for oxygen evolution reaction, ACS Appl. Nano Mater. 2 (2019) 744-749.

[18] F. Yin, G. Li, H. Wang, Hydrothermal synthesis of α-MnO_2/MIL-101 (Cr) composite and its bifunctional electrocatalytic activity for oxygen reduction/evolution reactions, Catal. Commun. 54 (2014) 17-21.

[19] D. Bélanger, T. Brousse, J. Long, Manganese oxides: battery materials make the leap to electrochemical capacitors, Electrochem. Soc. Interface 17 (2008) 49.

[20] A.M. Butt, S. Abbas, T. Noor, M.N. Tahir, E.U. Mughal, S.H. Sumrra, M.N. Zafar, New 3-D Mn (II) Coordination Polymer with Redox Active Oxalate Linker; An Efficient and Robust Electrocatalyst for Oxygen Evolution Reaction, Inorg. Chim. Acta (2020) 119982.

[21] M. Widelicka, P. Ławniczak, A. Pietraszko, K. Pogorzelec-Glaser, A. Łapiński, Investigation of the thermal and conductive properties of oxalic acid salts with planar and undulating proton-conducting layers, CrystEngComm 22 (2020) 2031-2041.

[22] L. Wang, Y. Wu, R. Cao, L. Ren, M. Chen, X. Feng, J. Zhou, B. Wang, Fe/Ni Metal–Organic Frameworks and Their Binder-Free Thin Films for Efficient Oxygen Evolution with Low Overpotential, ACS Appl. Mater. Interfaces 8 (2016) 16736-16743.

[23] S. Ibrahim, K. Shehzadi, B. Iqbal, S. Abbas, D.R. Turner, M.A. Nadeem, A trinuclear cobalt-based coordination polymer as an efficient oxygen evolution electrocatalyst at neutral pH, J. Colloid Interface Sci. 545 (2019) 269-275.

[24] S. Ibrahim, Y. Cheng, D. Zhao, M.A. Nadeem, A new insight for photocatalytic hydrogen production by a Cu/Ni based cyanide bridged polymer as a co-catalyst on titania support in glycerol water mixture, Int. J. Hydrogen Energy 44 (2019) 2508-2518.

[25] S. Maji, I. López, F. Bozoglian, J. Benet-Buchholz, A. Llobet, Mononuclear ruthenium–water oxidation catalysts: discerning between electronic and hydrogen-bonding effects, Inorg. Chem. 52 (2013) 3591-3593.

[26] D.C. Marelius, S. Bhagan, D.J. Charboneau, K.M. Schroeder, J.M. Kamdar, A.R. McGettigan, B.J. Freeman, C.E. Moore, A.L. Rheingold, A.L. Cooksy, How Do Proximal Hydroxy or Methoxy Groups on the Bidentate Ligand Affect [(2, 2′; 6′, 2"-Terpyridine) Ru (N, N)X] Water-Oxidation Catalysts? Synthesis, Characterization, and Reactivity at Acidic and Near-Neutral pH, Eur. J. Inorg. Chem. 2014 (2014) 676-689.

[27] X. Zheng, L. Yu, B. Lan, G. Cheng, T. Lin, B. He, W. Ye, M. Sun, F. Ye, Three-dimensional radial α-MnO_2 synthesized from different redox potential for bifunctional oxygen electrocatalytic activities, J. Power Sources 362 (2017) 332-341.

[28] M. Jahan, S. Tominaka, J. Henzie, Phase pure α-Mn_2O_3 prisms and their bifunctional electrocatalytic activity in oxygen evolution and reduction reactions, Dalton Trans. 45 (2016) 18494-18501.

[29] A. Indra, P.W. Menezes, I. Zaharieva, E. Baktash, J. Pfrommer, M. Schwarze, H. Dau, M. Driess, Active Mixed-Valent MnO_x Water Oxidation Catalysts through Partial Oxidation (Corrosion) of Nanostructured MnO Particles, Angew. Chem. Int. Ed. 52 (2013) 13206-13210.

[30] K. Selvakumar, S.M.S. Kumar, R. Thangamuthu, P. Rajput, D. Bhattacharyya, S.N. Jha, 2D and 3D Silica-Template-Derived MnO_2 Electrocatalysts towards Enhanced Oxygen Evolution and Oxygen Reduction Activity, ChemElectroChem 5 (2018) 3980-3990.

[31] Y. Li, B. Jia, B. Chen, Q. Liu, M. Cai, Z. Xue, Y. Fan, H.-P. Wang, C.-Y. Su, G. Li, MOF-derived Mn doped porous CoP nanosheets as efficient and stable bifunctional electrocatalysts for water splitting, Dalton Trans. 47 (2018) 14679-14685.

[32] D. Li, H. Baydoun, C.u.N. Verani, S.L. Brock, Efficient water oxidation using CoMnP nanoparticles, J. Am. Chem. Soc. 138 (2016) 4006-4009.

[33] M. Kölbach, S. Fiechter, R. van de Krol, P. Bogdanoff, Evaluation of electrodeposited α-Mn_2O_3 as a catalyst for the oxygen evolution reaction, Catal. Today 290 (2017) 2-9.

[34] I. Zaharieva, P. Chernev, M. Risch, K. Klingan, M. Kohlhoff, A. Fischer, H. Dau, Electrosynthesis, functional, and structural characterization of a water-oxidizing manganese oxide, Energy Environ. Sci. 5 (2012) 7081-7089.

[35] T. Takashima, K. Hashimoto, R. Nakamura, Mechanisms of pH-dependent activity for water oxidation to molecular oxygen by MnO_2 electrocatalysts, J. Am. Chem. Soc. 134 (2012) 1519-1527.

[36] H. Liu, X. Gao, X. Yao, M. Chen, G. Zhou, J. Qi, X. Zhao, W. Wang, W. Zhang, R. Cao, Manganese (II) phosphate nanosheet assembly with native out-of-plane Mn centres for electrocatalytic water oxidation, Chem. Sci. 10 (2019) 191-197.

[37] D. Jeong, K. Jin, S.E. Jerng, H. Seo, D. Kim, S.H. Nahm, S.H. Kim, K.T. Nam, Mn_5O_8 nanoparticles as efficient water oxidation catalysts at neutral pH, ACS Catal. 5 (2015) 4624-4628.

[38] T.-X. Lan, W.-S. Gao, C.-N. Chen, H.-S. Wang, M. Wang, Y.-h. Fan, Two tetranuclear 3d–4f heterometal complexes Mn_2Ln_2 (Ln= Dy, Gd): synthesis, structure, magnetism, and electrocatalytic reactivity for water oxidation, New J. Chem. 42 (2018) 5798-5805.

[39] Y. Gorlin, T.F. Jaramillo, A bifunctional nonprecious metal catalyst for oxygen reduction and water oxidation, J. Am. Chem. Soc. 132 (2010) 13612-13614.

[40] H.S. Jeon, S.J. Ahn, M.S. Jee, S.S. Yoon, Y.J. Hwang, B.K. Min, Water oxidation by manganese oxide electrocatalytic films synthesized by chemical solution deposition method, J. Electrochem. Soc. 163 (2016) F3113.

[41] M. Fekete, R.K. Hocking, S.L. Chang, C. Italiano, A.F. Patti, F. Arena, L. Spiccia, Highly active screen-printed electrocatalysts for water oxidation based on β-manganese oxide, Energy Environ. Sci. 6 (2013) 2222-2232.

[42] K. Jin, H. Seo, T. Hayashi, M. Balamurugan, D. Jeong, Y.K. Go, J.S. Hong, K.H. Cho, H. Kakizaki, N.g. Bonnet-Mercier, Mechanistic investigation of water oxidation catalyzed by uniform, assembled MnO nanoparticles, J. Am. Chem. Soc. 139 (2017) 2277-2285.

[43] C.-H. Kuo, I.M. Mosa, S. Thanneeru, V. Sharma, L. Zhang, S. Biswas, M. Aindow, S.P. Alpay, J.F. Rusling, S.L. Suib, Facet-dependent catalytic activity of MnO electrocatalysts for oxygen reduction and oxygen evolution reactions, Chem. Commun., 51 (2015) 5951-5954.

[44] X. Yu, M. Zhang, W. Yuan, G. Shi, A high-performance three-dimensional Ni–Fe layered double hydroxide/graphene electrode for water oxidation, J. Mater. Chem. A, 3 (2015) 6921-6928.

[45] T. Takashima, K. Hashimoto, R. Nakamura, Inhibition of charge disproportionation of MnO_2 electrocatalysts for efficient water oxidation under neutral conditions, J. Am. Chem. Soc. 134 (2012) 18153-18156.

[46] K. Jin, J. Park, J. Lee, K.D. Yang, G.K. Pradhan, U. Sim, D. Jeong, H.L. Jang, S. Park, D. Kim, Hydrated manganese (II) phosphate ($Mn_3(PO_4)_2 \cdot 3H_2O$) as a water oxidation catalyst, J. Am. Chem. Soc. 136 (2014) 7435-7443.

[47] J. Park, H. Kim, K. Jin, B.J. Lee, Y.-S. Park, H. Kim, I. Park, K.D. Yang, H.-Y. Jeong, J. Kim, A new water oxidation catalyst: lithium manganese pyrophosphate with tunable Mn valency, J. Am. Chem. Soc. 136 (2014) 4201-4211.

[48] B. Zhang, H. Chen, Q. Daniel, B. Philippe, F. Yu, M. Valvo, Y. Li, R.B. Ambre, P. Zhang, F. Li, Defective and “c-disordered” Hortensia-like layered MnO_x as an efficient electrocatalyst for water oxidation at neutral pH, ACS Catal. 7 (2017) 6311-6322.

[49] K. Mette, A. Bergmann, J.P. Tessonnier, M. Hävecker, L. Yao, T. Ressler, R. Schlögl, P. Strasser, M. Behrens, Nanostructured manganese oxide supported on carbon nanotubes for electrocatalytic water splitting, ChemCatChem 4 (2012) 851-862.